Supporting Information

Spontaneous and Directional Bubble Transport on Porous Copper Wires with Complex Shapes in Aqueous Media

Wenjing Li[†, ‡], *Jingjing Zhang*[†, ‡], *Zhongxin Xue*[§], *Jingming Wang*[†,*], *and Lei Jiang*[†,#]

[†] Key Laboratory of Bio-Inspired Smart Interfacial Science and Technology of Ministry of Education, School of Chemistry and Environment, Beihang University, Beijing, 100191, P.R. China

[#] Laboratory of Bio-inspired Smart Interface Science, Technical Institute of Physics and Chemistry, Chinese Academy of Science, Beijing, 100190, P. R. China

[§]School of Chemistry and Materials Science, Ludong University, Yantai, 264025, P.R. China

E-mail: wangjm@buaa.edu.cn Give contact information for the author(s) to whom correspondence should be addressed.

S1 The effect of tilt angles of the whole copper wires on the gas bubble transportation

The tilt angles of the whole copper wires greatly influenced the gas bubble transportation. When the tilt angle is larger than 0°, the buoyance force on all the parts of the complex-shaped is larger than 0. The complement of buoyance force along the copper wire has great influence on gas bubble transportation direction. We found that the bubble transport direction changed when the tilt angle changed to 90°. The direction of gas bubble transportation is from the bubbles at the base part to the ones at the top part, no mater the gas bubbles at the top part is larger than that on the base or not. Even a single gas bubble at the base part transported automatically to the top part. Similar phenomena are found on the copper cones with rectangle, wave and helix shape, as illustrated in Figures S1, S2 and S3.

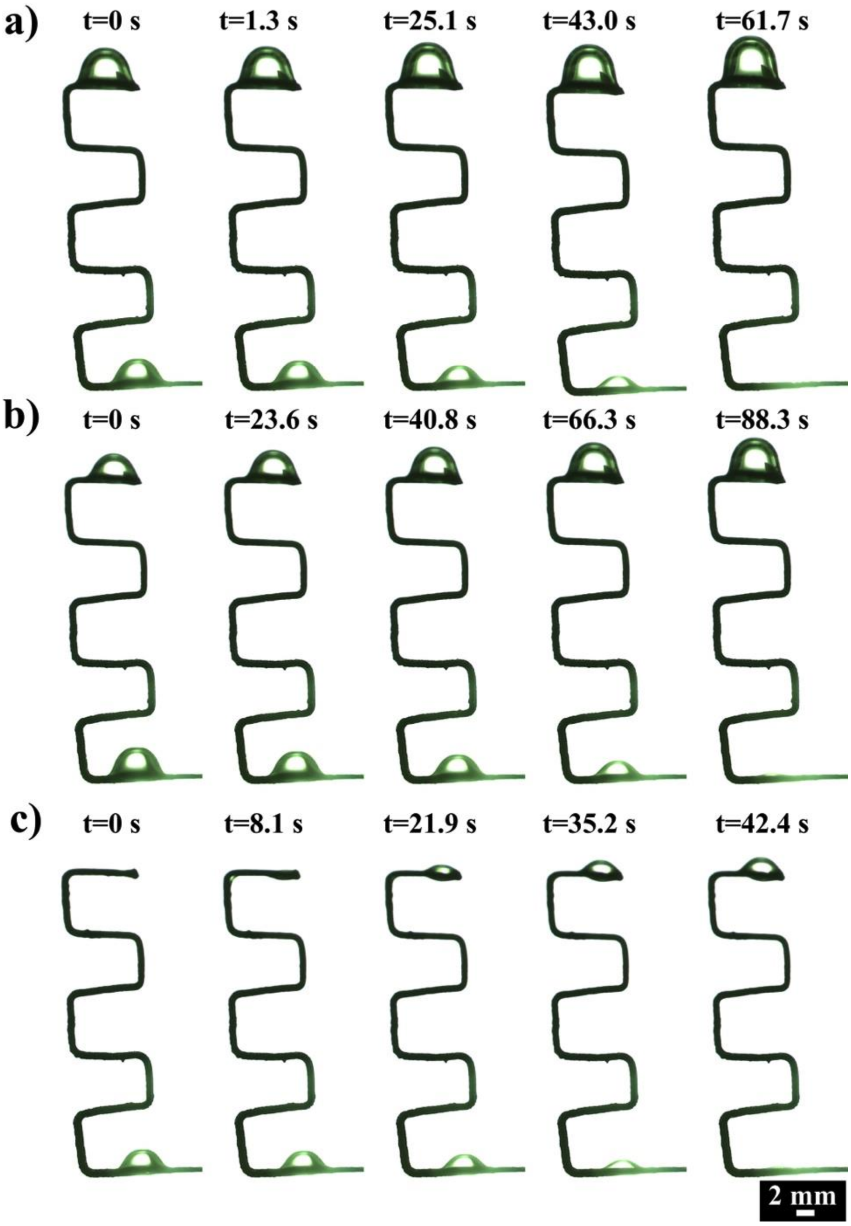

Figure S1 Microscopic observations of the directional transport of gas bubbles on the rectangle-shaped copper wire surface with the tilt angle of 90° underwater. Transport direction: (a) from small bubble at base part to large bubble at top part; (b) from large bubble at the base part to small bubble at the top part; (c) a gas bubble at the base part transported automatically to the top part.

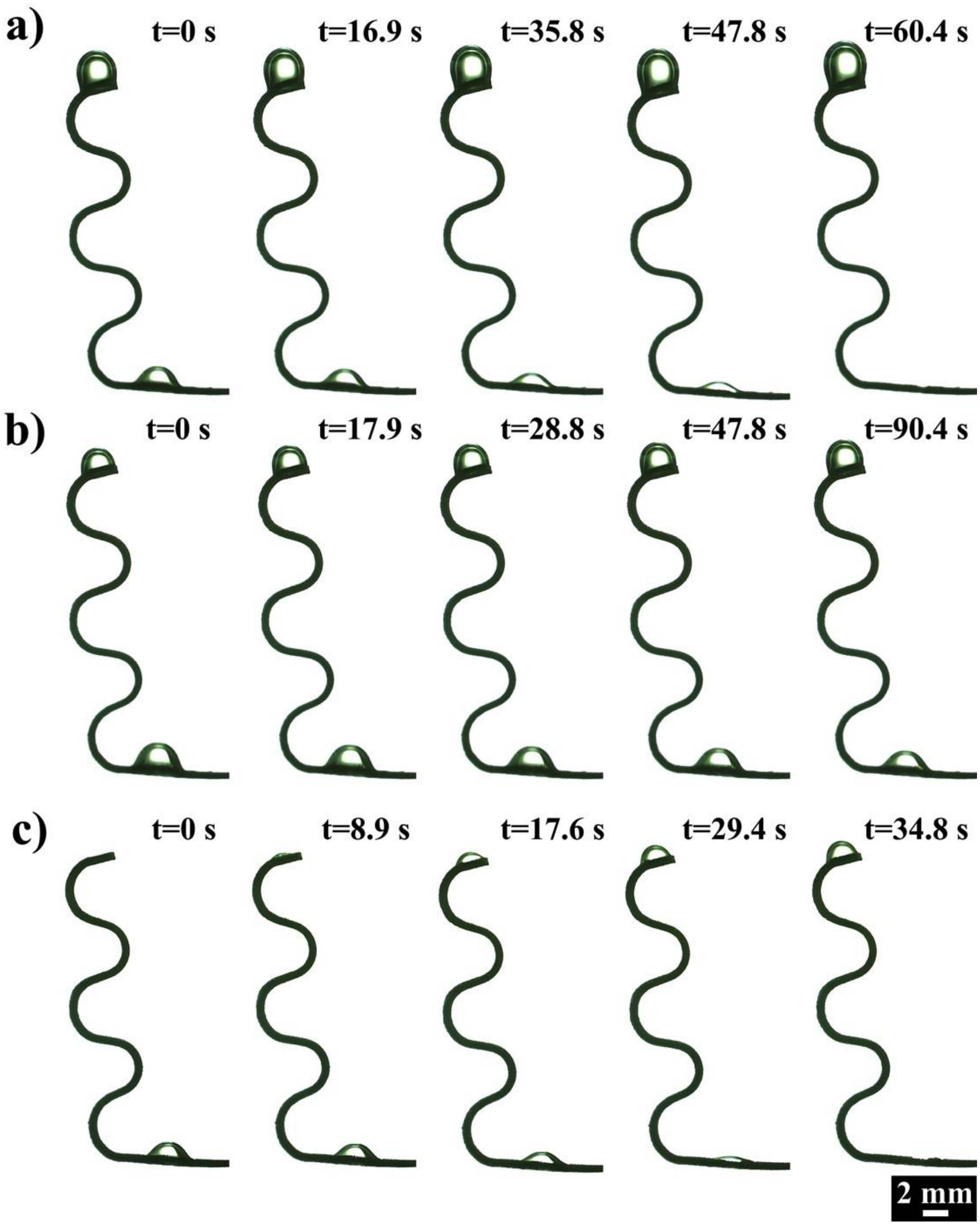

Figure S2 Microscopic observations of the directional transport of gas bubbles on the wave-shaped copper wire surface with the tilt angle of 90° underwater. Transport direction (a) from small bubble at base part to large bubble at top part; (b) from large bubble at the base part to small bubble at the top part; (c) a gas bubble at the base part transported automatically to the top part.

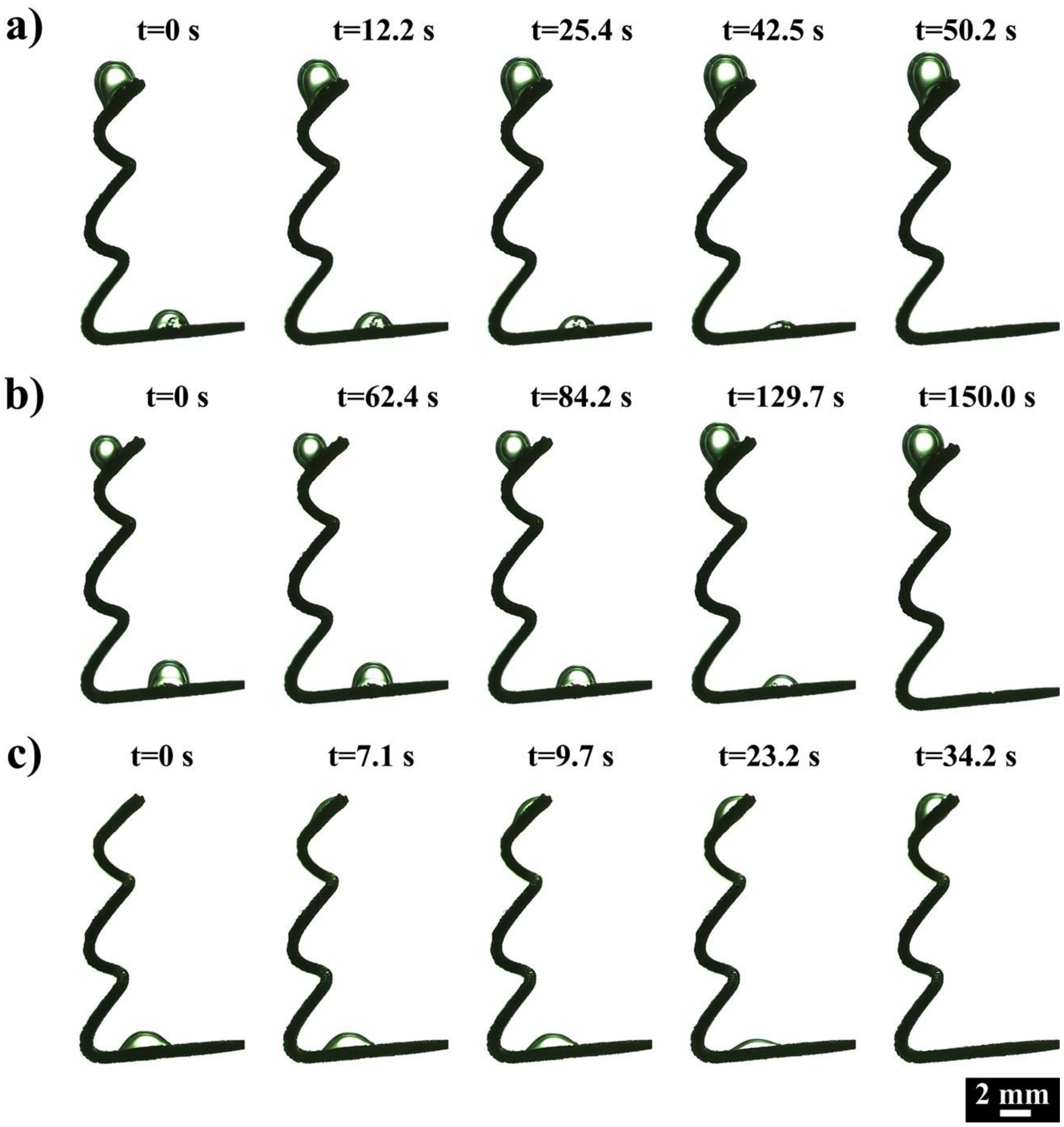

Figure S3 Microscopic observations of the directional transport of gas bubbles on the helix-shaped copper wire surface with the tilt angle of 90° underwater. Transport direction (a) from small bubble at base part to large bubble at top part; (b) from large bubble at the base part to small bubble at the top part; (c) a gas bubble at the base part transported automatically to the top part.

Video 1. Microscopic observations of the directional gas bubbles transport on the copper wire interface with rectangle shape (Left: 3 μL; Right: 5 μL)

Video 2. Microscopic observations of the directional gas bubbles transport on the copper wire interface with wave shape (Left: 3 μL; Right: 5 μL)

Video 3. Microscopic observations of the directional gas bubbles transport on the copper wire interface with helix shape (Left: 3 μL; Right: 5 μL)

S2

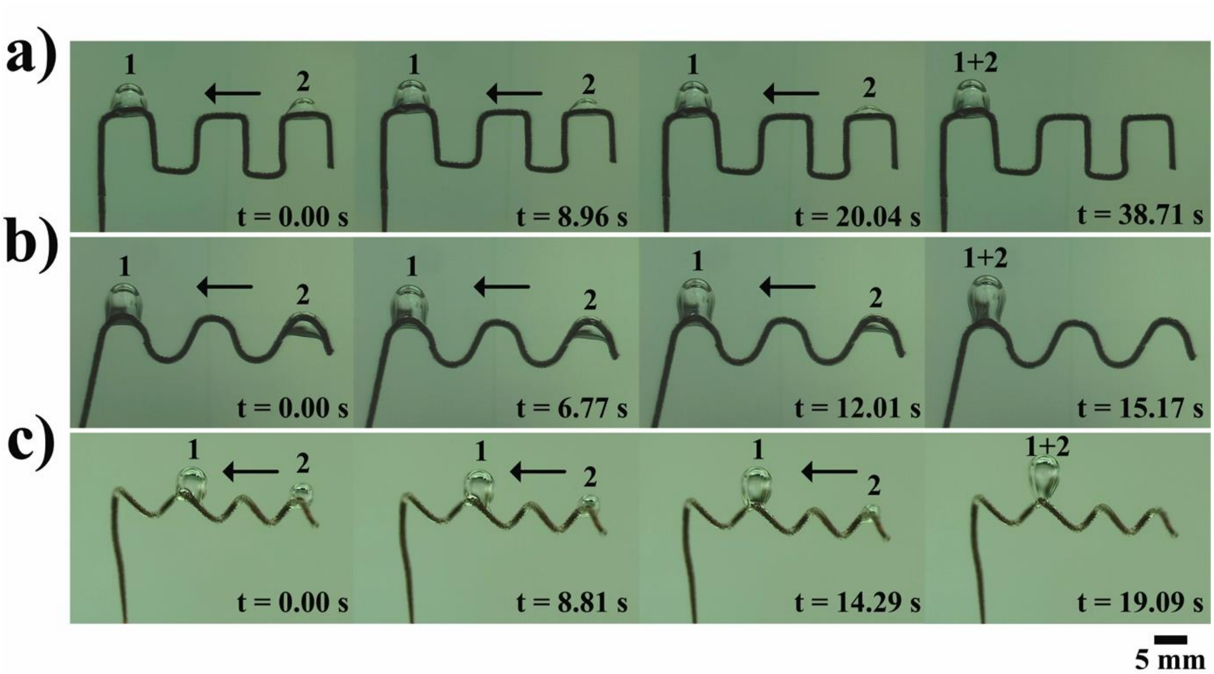

Figure S4 Microscopic observations of the directional gas bubbles (t) transported on the copper wire interfaces with a) rectangle, b) wave, and c) helix shapes (Left: a large bubble; Right: a small bubble). Regardless of shape, the coppers wires captured and directionally transported gas bubbles, and the gas transportation direction was always toward to the larger bubble.

S3 The difference of the bubble size will initiate the transportation

It is impossible to get two bubbles with the identical size. Even though there is a tiny difference between two bubbles, the difference of Laplace pressure can drive the small bubble to move slowly toward the big one. Then the differences between the two bubbles becomes larger and larger, and the transportation speed becomes faster and faster. Finally, the small one will coalesce with the large one to become a larger bubble (as shown in **Figure S5**). That is to say, a tiny difference of two bubbles will initiate the transportation.

Comparing with the contribution of the difference of bubble size, the effect of the distance between two bubbles effect on the initiation of the gas bubble transportation was not found. In our experiments, the cooper wire was only 35-80 mm long. The distance between two bubbles may have an effect on the mass transfer if it is long enough. Therefore, in this manuscript, the effect of distance between two bubbles on bubble transport direction can be neglected.

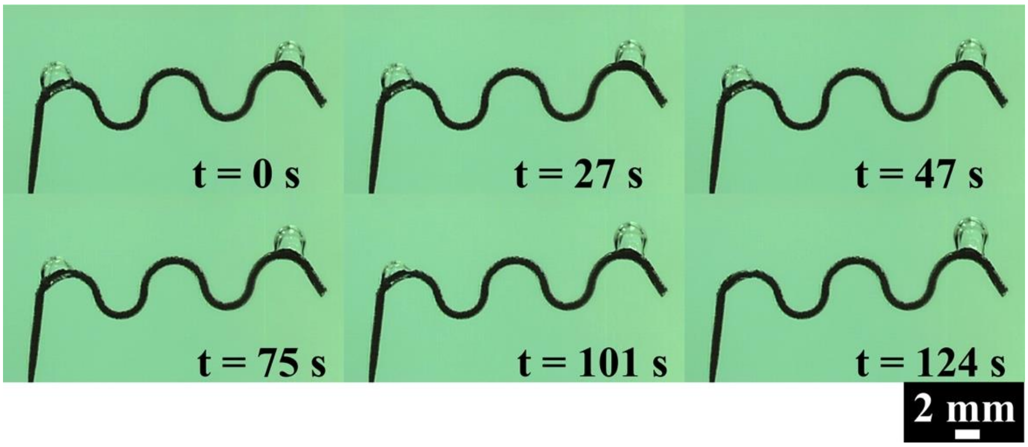

Figure S5 Microscopic observations of the directional transport of two bubbles with similar volume on the copper wire surface underwater (the volume of two bubble is 3 μL).

S4 Gas bubble transport process between three bubbles with different volumes

We investigated the transport phenomena among three gas bubbles with the volume of 2, 3 and 4 μL. As depicted in Figure S6a, three bubbles with the size of 2 (bubble 1), 3 (bubble 2), and 4 μL (bubble 3) were attached on the copper wire with same spacing from left to right in an aqueous medium, bubble 2 transferred to bubble 3, while bubble 1 transferred to bubble 2 and then to bubble 3. After bubble 1 was carried away completely, the transportation process is from the small one (bubble 2a+1a) to the large one (bubble 3+2b+1b).

If three bubbles with the size of 3 (bubble 2), 2 (bubble 1), and 4 μL (bubble 3) were attached on the copper wire from left to right with same spacing in an aqueous medium. We found that the gas bubbles transportation can be divided into two stages. At the first stage, bubble 1 was transferred to bubble 3 and to bubble 2 at the same time, because of the different

Laplace pressures (between bubble 1 and 2 and between bubble 1 and 3). After bubble 1 transported completely, the transportation process is from the small one (bubble 2+1a) to the large one (bubble 3+1b), which is similar to the transportation process of two bubbles, as shown in Figure S6b. If the bubble with the size of 4 μL (bubble 3) was attached between the two bubbles with the size of 2 (bubble 1) and 3 μL (bubble 2) on the copper wire (with same spacing) in an aqueous medium, both of bubble 1 and bubble 2 transferred to bubble 3. However, if the largest bubble (bubble 3) was in the middle of the three bubbles, the bubble 1 could not transfer to bubble 2. After bubble 1 transported completely, the transportation process is from the small one (bubble 2) to the large one (bubble 3+1), as shown in Figure S6c.

In summary, if three bubbles with different sizes were attached on the copper wire, the smallest one transported firstly, and then the second large one transported completely. Finally, the three bubbles coalesce to form one bubble at the position of the largest one. That is to say, the bubble transportation direction is always towards to the largest bubble.

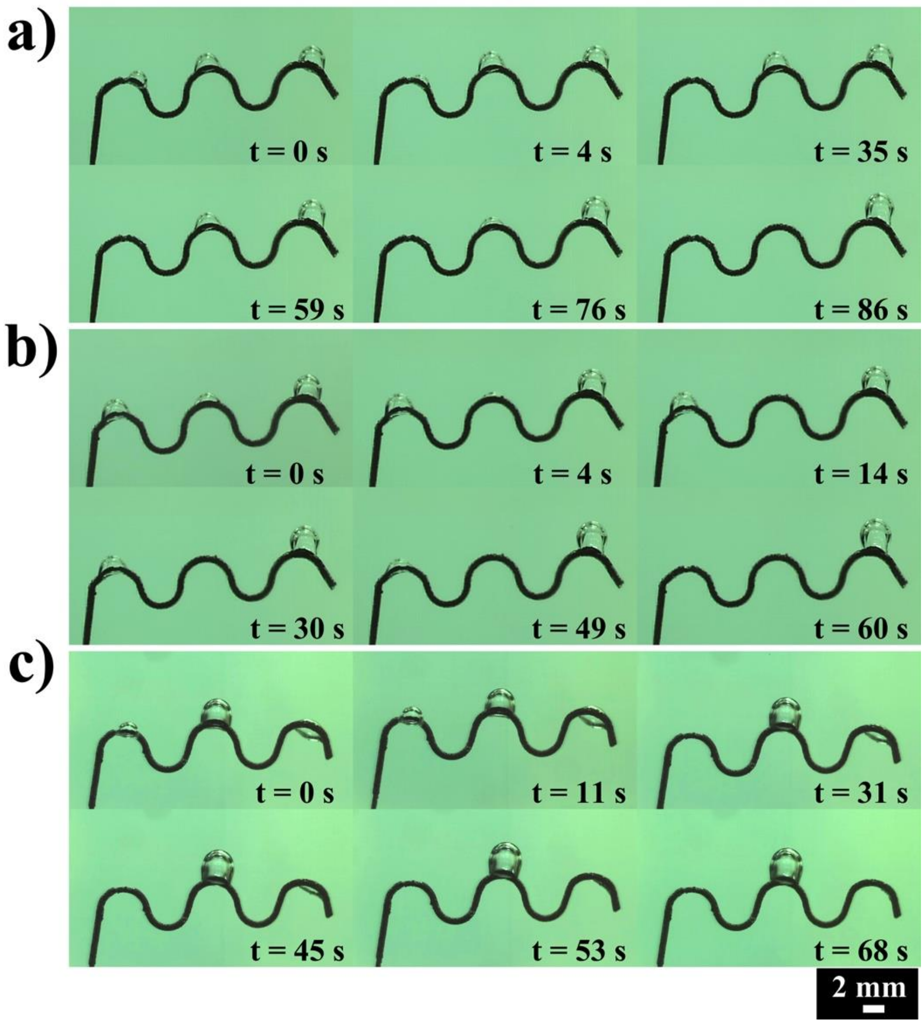

Figure S6 Microscopic observations of the directional transport of three gas bubbles with different volumes.

S5 The effect of a continuous gas film on gas transport

We have made a copper wire with a smooth band between (Figure S7a). SEM image showed a clear junction between the smooth band and the rough region with 3D porous structure (Figure S7b). We found that the smooth band blocked the bubble transport (Figure S7c). Therefore, a continuously rough region is necessary to form a continuous gas film for gas transport.

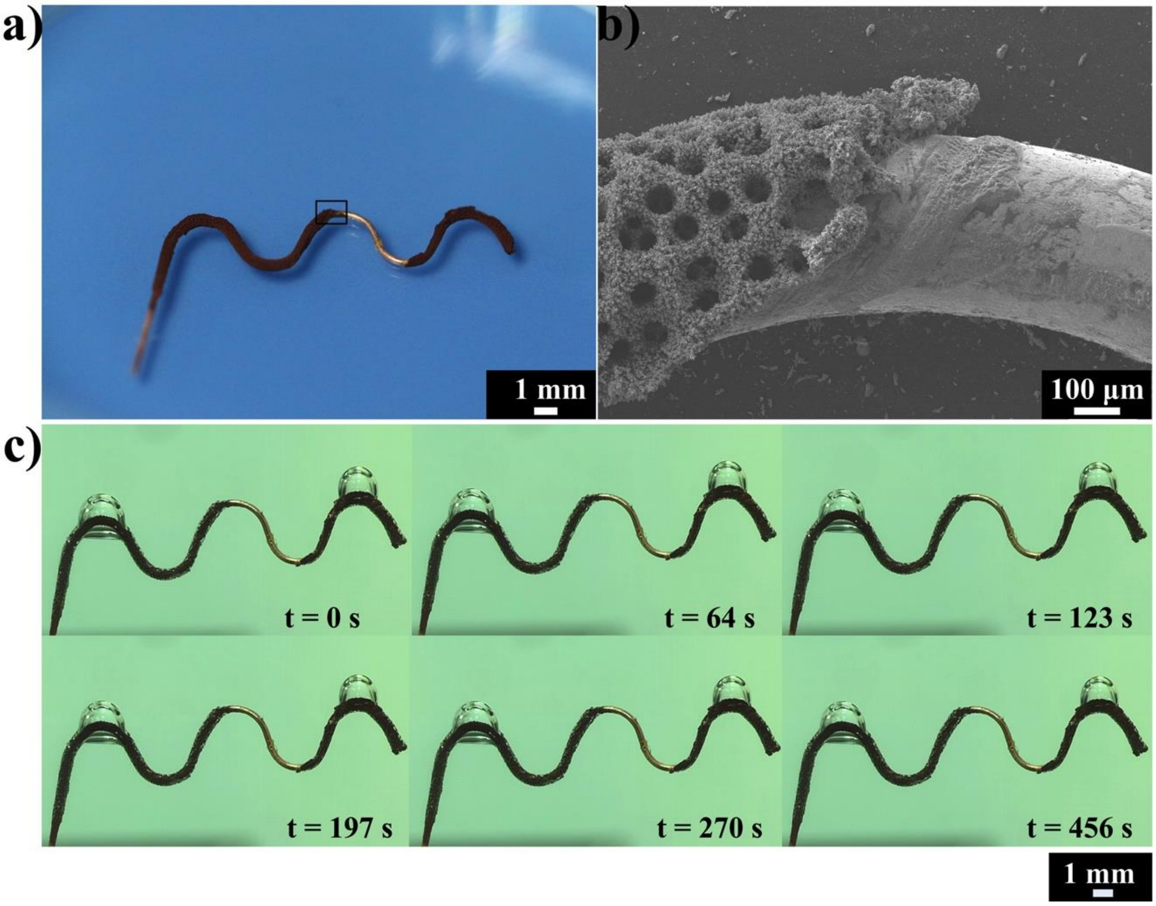

Figure S7 Gas bubble transport phenomenon on a wave-shaped cooper wire with a smooth band between. (a) Photograph of a wave-shaped cooper wire with a smooth band between; (b) SEM image showed a clear junction between the smooth band and the rough region with 3D porous structure; (c) Microscopic observations of the directional transport of two gas bubbles blocked by the smooth band.

S6 The effect of the Laplace pressure on the speed of gas bubble transport on wave-shaped copper wire

We studied the influence of Laplace pressure on the speed of gas bubble transport. We kept the size of small bubbles in the same scale (3 μL) and the size of large bubbles changed from 5 to 11 μL. We found that the average speed increased with the increase of the Laplace pressure on the rectangle- (Figures S9), wave- (Figure S10) and helix-shaped (Figure S11) copper wires.

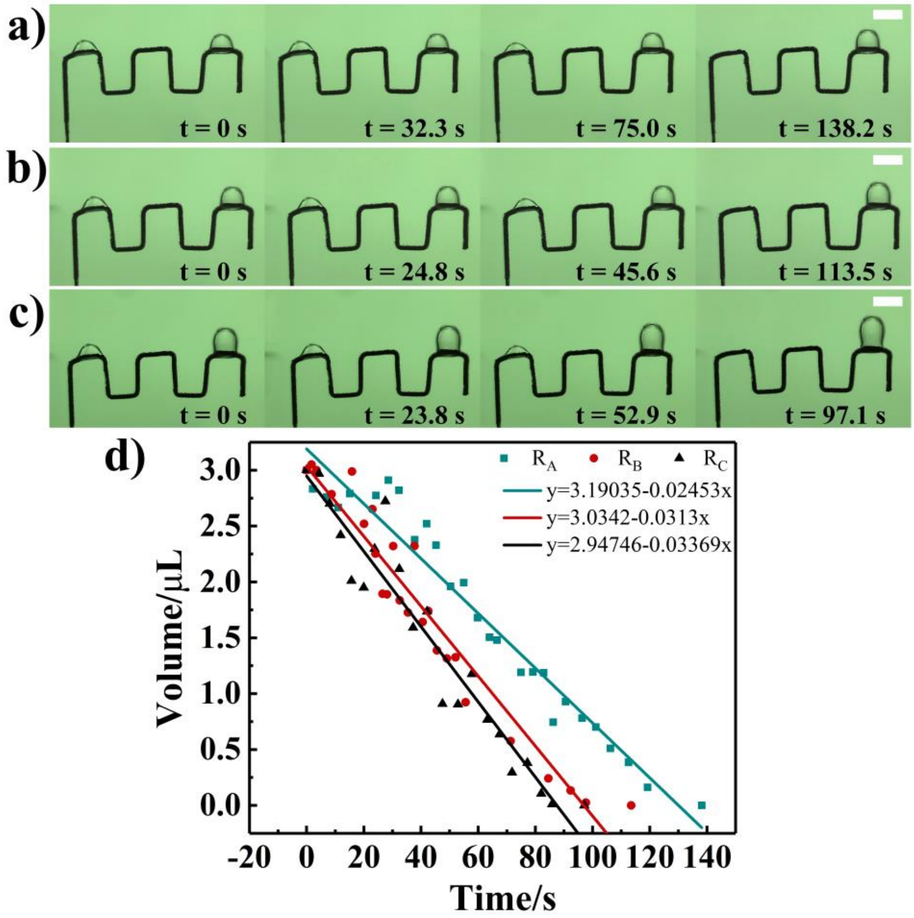

Figure S8 Microscopic observations of the directional transport of two bubbles with different Laplace pressure on the rectangle shaped copper. Regardless of the Laplace pressure, the coppers wires captured and directionally transported gas bubbles, and the gas transportation direction was always from small bubbles to larger ones. Small bubbles: 3 μL; Large bubbles: (a) R_A: 5 μL; (b) R_B: 8 μL; (c) R_C: 11 μL. Scale bar: 5 mm. (d) The volume variations of gas bubbles that transported to the target gas bubbles with different Laplace pressure on the rectangle-shaped copper wires.

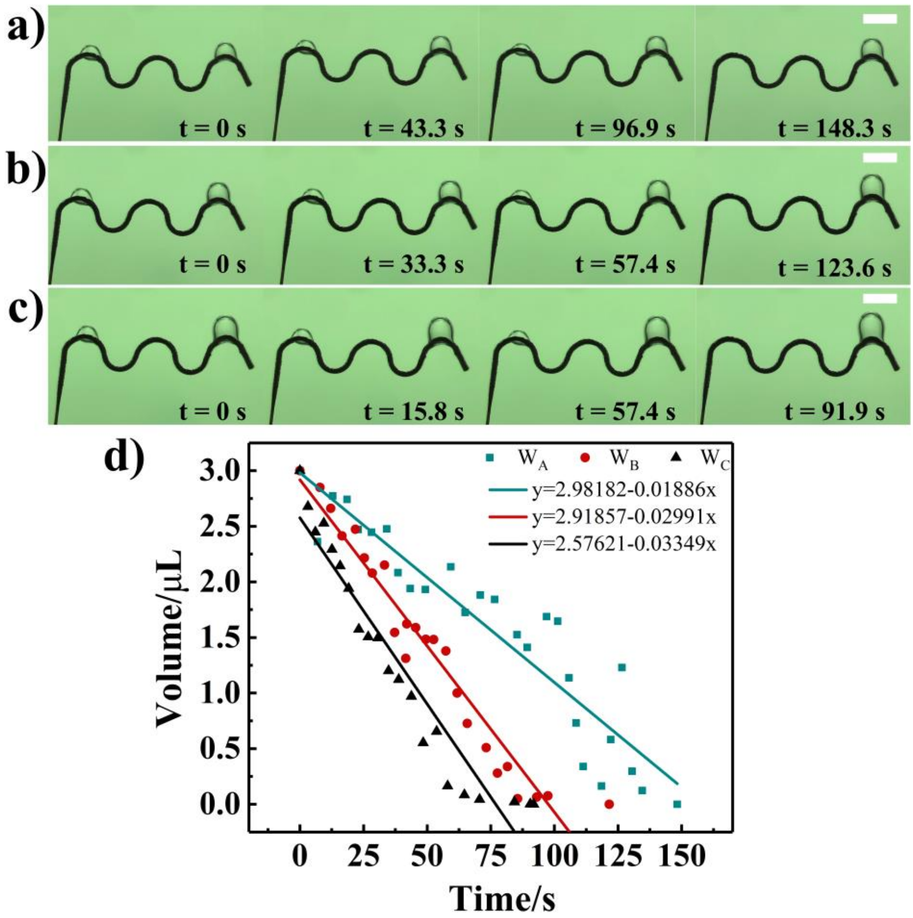

Figure S9 Microscopic observations of the directional transport of two bubbles with different Laplace pressure on the wave shaped copper. Regardless of the Laplace pressure, the coppers wires captured and directionally transported gas bubbles, and the gas transportation direction was always from small bubbles to larger ones. Small bubbles: 3 μL; Large bubbles (a) W_A: 5 μL; (b) W_B: 8 μL; (c) W_C: 11 μL. Scale bar: 5 mm. (d) The volume variations of gas bubbles that transported to the target gas bubbles with different Laplace pressure on the wave-shaped copper wires.

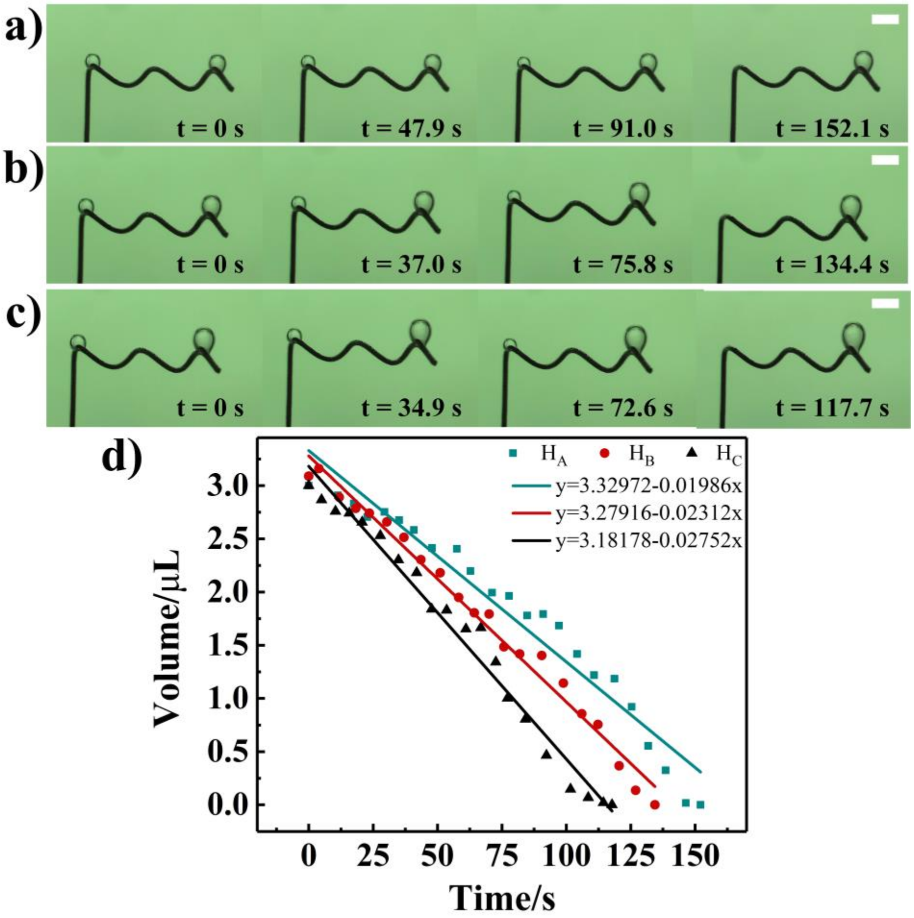

Figure S10 Microscopic observations of the directional transport of two bubbles with different Laplace pressure on the helix shaped copper. Regardless of the Laplace pressure, the coppers wires captured and directionally transported gas bubbles, and the gas transportation direction was always from small bubbles to larger ones. Small bubbles: 3 μL ; Large bubbles (a) H_A: 5 μL; (b) H_B: 8 μL; (c) H_C: 11 μL. Scale bar: 5 mm. (d) The volume variations of gas bubbles that transported to the target gas bubbles with different Laplace pressure on the helix-shaped copper wires.

S7 The effect of the channel length on the speed of gas bubble transport on wave-shaped copper wire

We investigated the effect of the channel length on the speed of gas bubble transport on wave-shaped copper wire. We found that the average transport speed of gas bubbles increased with the decrease of the distances between two bubbles (Figure S11).

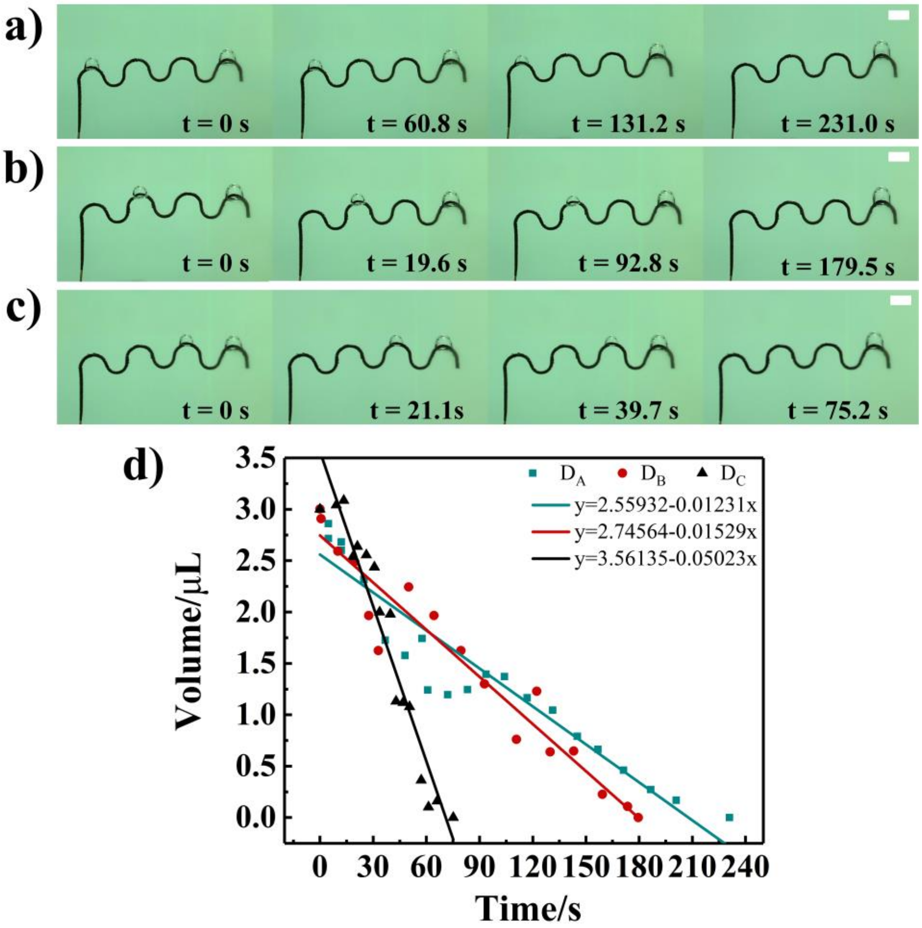

Figure S11 Microscopic observations of the directional transport between two bubbles with different distances on the wave shaped copper. Regardless of the distances between two bubbles, the coppers wires captured and directionally transported gas bubbles, and the gas transportation direction was always from small bubbles to larger ones. Small bubbles: 3 μL; large bubbles (a) D_A: 3 wave cycles; (b) D_B: 2 wave cycles; (c) 1 wave cycle. Scale bar: 5 mm. (d) The volume variations of gas bubbles that transported to the target gas bubbles with different distances on the wave-shaped copper wires.

S8 The effect of the thickness of trapped gas layers on gas bubble transport

The thickness of gas layers trapped on the shaped wires is summarized by the thickness and the average size of the 3D porous structures. The thickness and the average size of the 3D porous structures can be regulated by the deposition times and current density. Both of the thickness and the average size of the 3D porous structures increased with the deposition times and current density. Thus, the thickness of the gas layer increased with the deposition times and current density as well (*Adv. Mater.* 2015, 27, 2384).

We used three different groups of deposition times and current density. Group 1, deposition times were changed (15, 30 and 45 s) at same current density of 0.60 A/cm^2 (Figure S12); Group 2, current density was changed (0.3, 0.6 and 0.9 A/cm^2) with deposition time of 45 s (Figure S13); Group 3, both of the current density and deposition time were changed from 0.3 A/cm^2 and 15 s, 0.6 A/cm^2 and 45 s, to 1.2 A/cm^2 and 60 s (Figure S14). We found that the time for gas bubbles transport decreased with the increase of the thickness of the 3D porous structures and the average surface pore size. The increase of the thickness and the average size of the 3D porous structures significantly increased the size of the channels for gas bubble transport. The increase of the channel sizes helped gas bubbles to improve their transport efficiency.

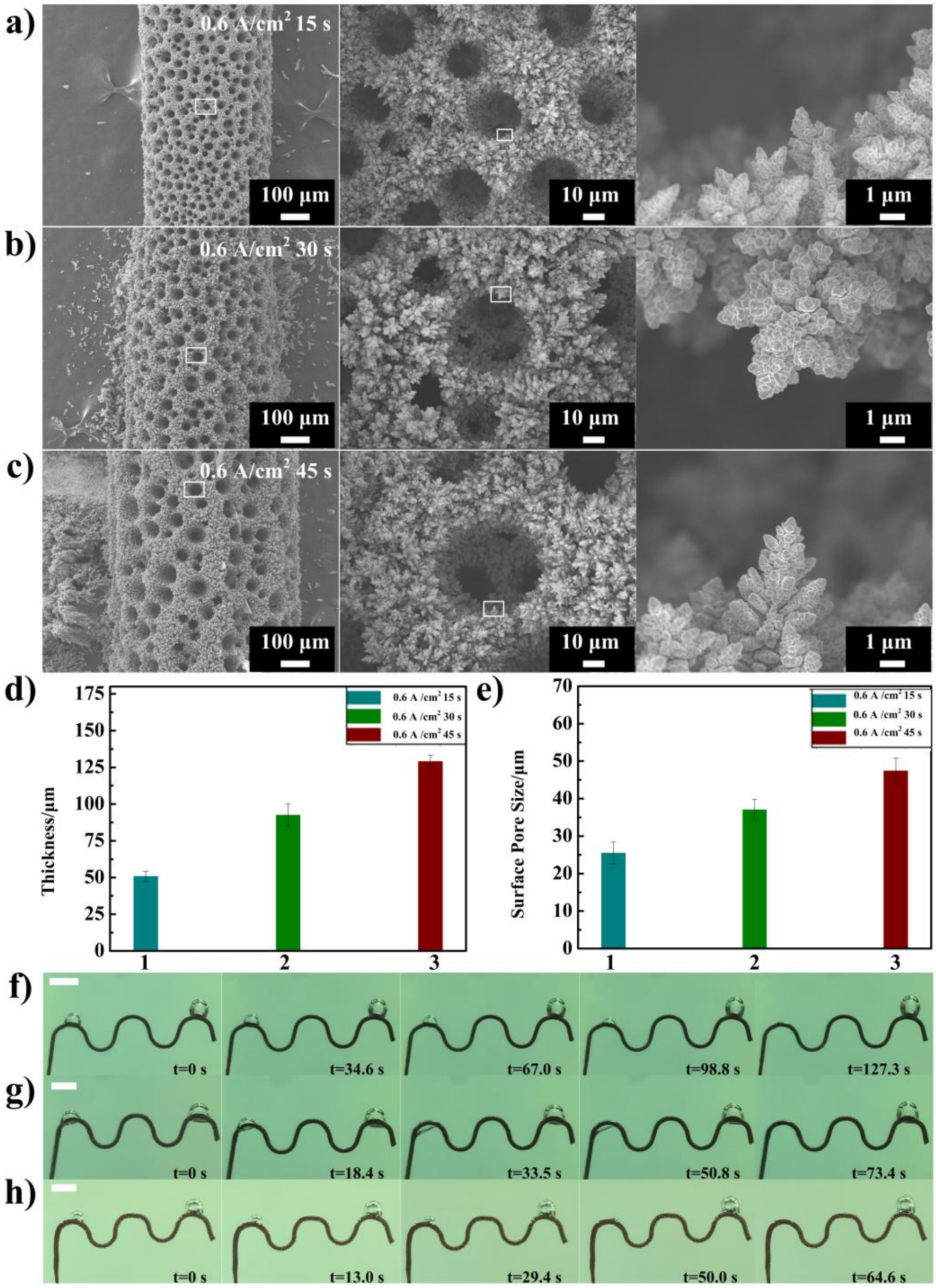

Figure S12 The effect of the thickness and the surface pore size on the gas bubble transport phenomena. SEM images of cooper wires prepared with deposition time of (a) 15, (b) 30 and (c) 45 s; (d) the thickness of the 3D porous structures; (e) the average surface pore size; Microscopic observations of the directional transport of gas bubbles on the wave-shaped copper wire surface prepared with deposition time of (f) 15, (g) 30 and (h) 45 s. Current density: 0.60 A/cm^2. Scale bar: 5 mm.

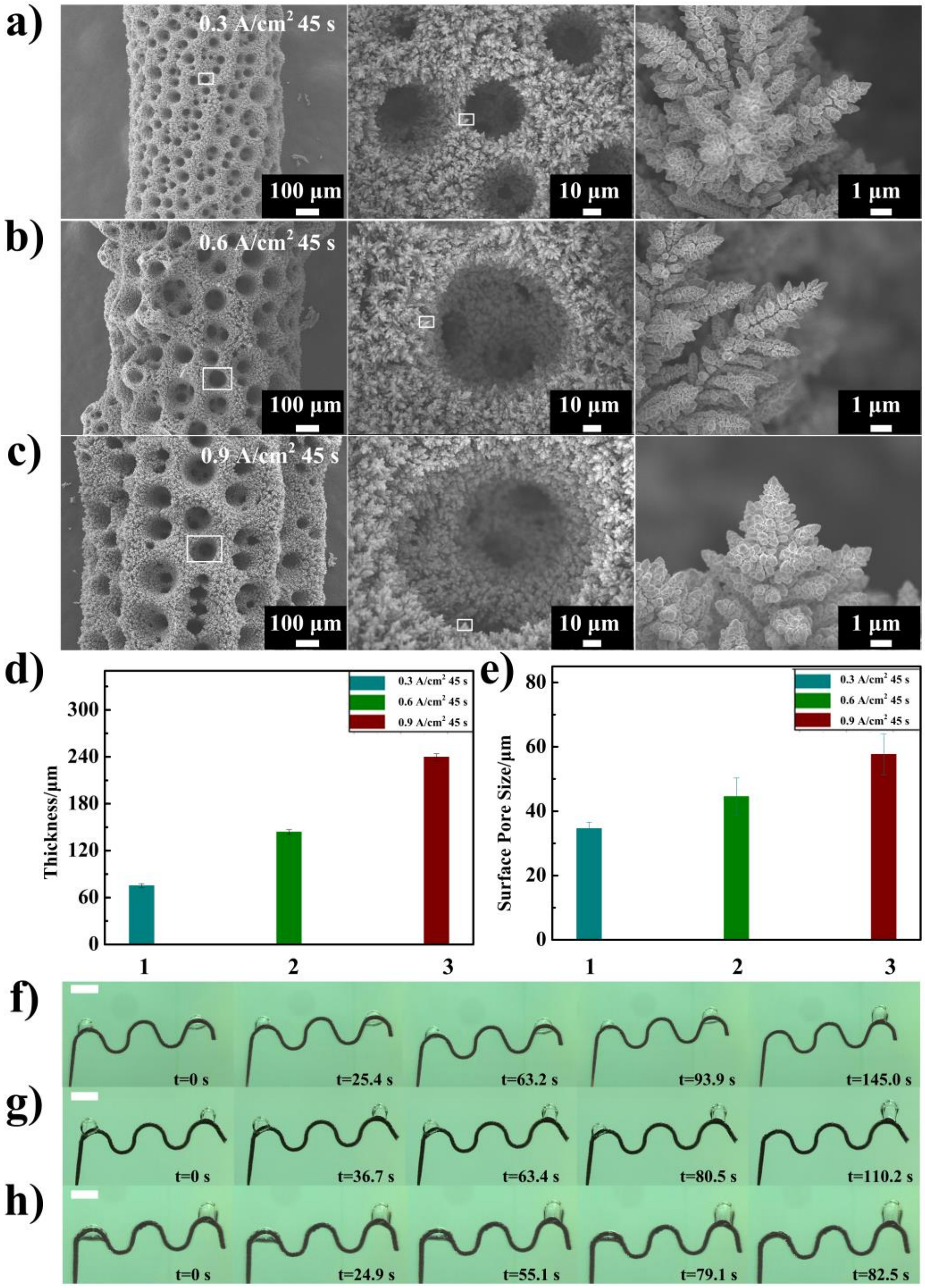

Figure S13 The effect of the thickness and the surface pore size on the gas bubble transport phenomena. SEM images of cooper wires prepared with current density of (a) 0.3, (b) 0.6 and (c) 0.9 A/cm^2; (d) the thickness of the 3D porous structures; (e) the average surface pore size; Microscopic observations of the directional transport of gas bubbles on the wave-shaped copper wire surface prepared with current density of (f) 0.3, (g) 0.6 and (h) 0.9 A/cm^2. Deposition time: 45 s. Scale bar: 5 mm.

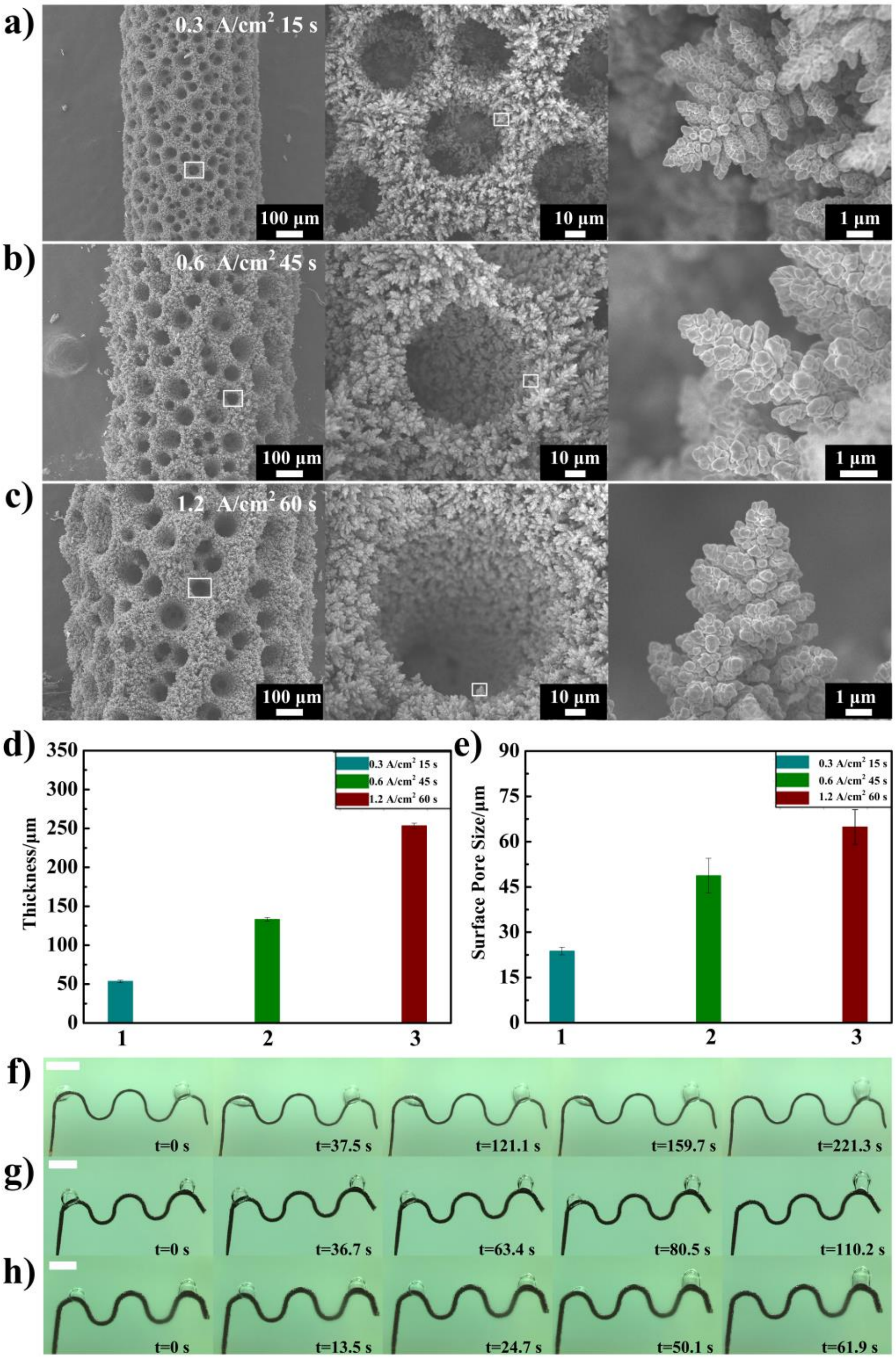

Figure S14 The effect of the thickness and the surface pore size on the gas bubble transport phenomena. SEM images of cooper wires prepared with current density and deposition time were changed from (a) 0.3 A/cm^2 and 15 s, (b) 0.6 A/cm^2 and 45 s, to (c) 0.9 A/cm^2 and 60 s; (d) the thickness of the 3D porous structures; (e) the average surface pore size; Microscopic observations of the directional transport of gas bubbles on the wave-shaped copper wire surface prepared with current density and deposition time were changed from (f) 0.3 A/cm^2 and 15 s, (g) 0.6 A/cm^2 and 45 s, to (h) 0.9 A/cm^2 and 60 s. Scale bar: 5 mm.

S9 Forces acting on the a rectangle shaped copper wire during immersion

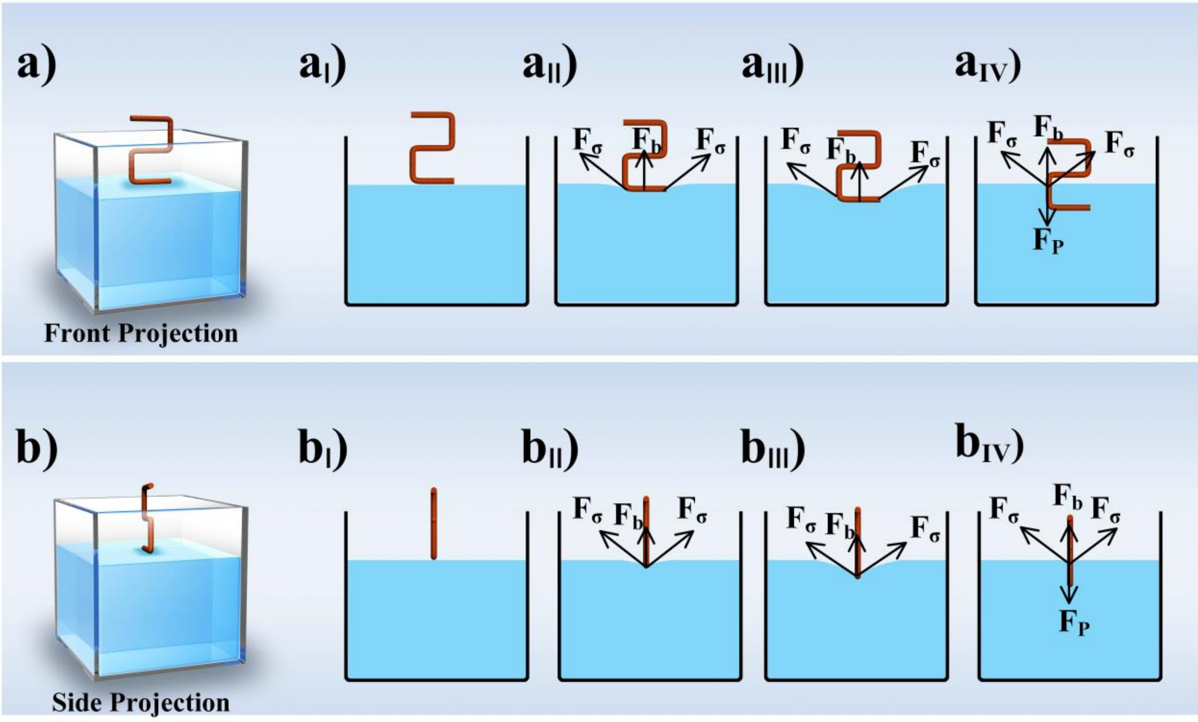

Figure S15 Schematic model the (a) front projunction and (b) side projunction of a rectangle shaped copper wire during immersion.

S10 The static contact angle images of water droplets and air bubbles on the copper wire interfaces with rectangle and helix shapes.

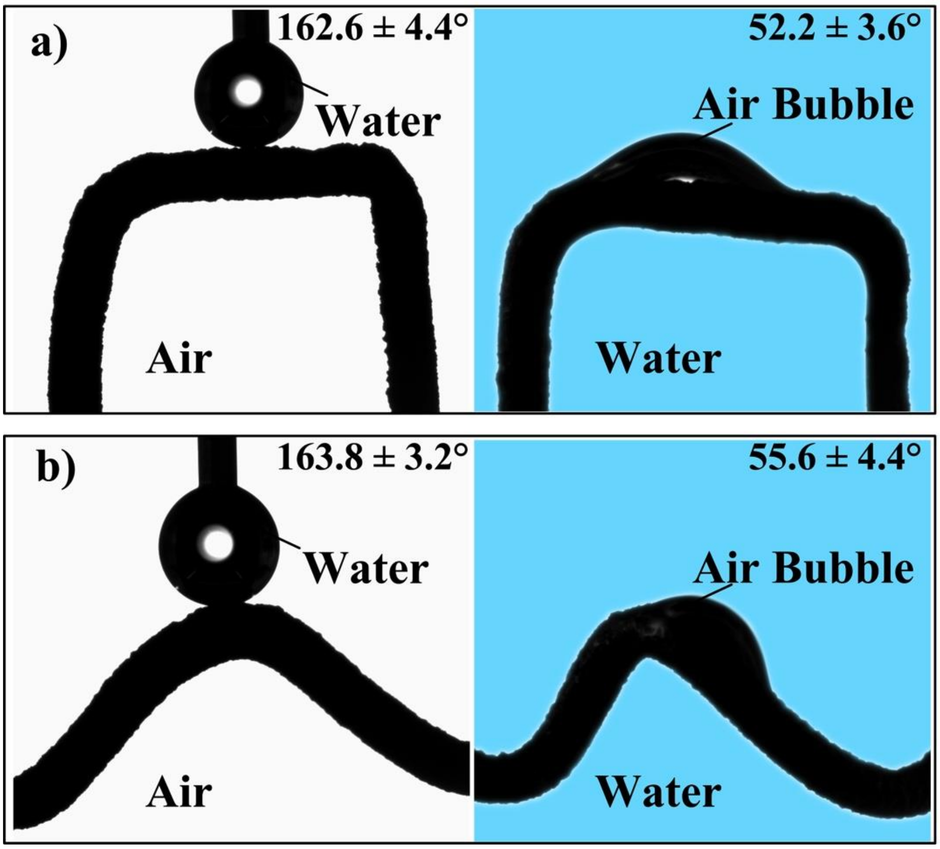

Figure S16 The static contact angle images of water droplets and air bubbles on the copper wire interfaces with rectangle (a) and helix (b) shapes.

S11 The analysis of the equilibrium state of gas bubbles on the copper wire

The equilibrium state of gas bubbles on the copper wire is analyzed as follows. The buoyancy force F_b exerted on spherical crown is proportional to the total volume V of the extruded liquid.

$$F_b = \rho g V$$

where $V = \frac{\rho}{3} h^2 \left(3R - h\right)$ and h=R+$R\ cos\Theta$=$R(1+cos\Theta)$

Here, R and h are the radius and height of the spherical crown, respectively. θ is the apparent contact angle of gas bubbles. Therefore, the buoyant force of gas bubbles is

$$F_b = \rho g V = \frac{\pi}{3} \rho g h^2 (3R - h)$$

$$= \frac{\pi}{3}\rho g R^2(1+\cos\theta)^2\,[3R - R(1+\cos\theta)]$$

$$= \frac{\pi}{3}\rho g R^3(1+\cos\theta)^2\,(2-\cos\theta)$$

Besides, across the liquid-gas interface of the spherical crown, there exists a Laplace force.

$$F_{Laplace} = \pi r^2 \frac{2\gamma}{R} = \pi R^2 \sin^2\theta \frac{2\gamma}{R} = 2\gamma\pi R \sin^2\theta$$

where the contact radius of the spherical crown r is equal to $\boldsymbol{R\sin\theta}$ ($r = R\sin\theta$).

When the buoyancy of the gas bubble balance the Laplace pressure, $F_b = F_{Laplace}$.

That is,

$$\frac{\pi}{3}\rho g R^3(1+\cos\theta)^2(2-\cos\theta) = 2\gamma\pi R\sin^2\theta$$

$$\rho g R^2(1+\cos\theta)^2(2-\cos\theta) = 6\gamma\sin^2 = 6\gamma(1-\cos^2\theta)$$

$$\because \sin\theta = \frac{2\tan\frac{\theta}{2}}{1+\tan^2\frac{\theta}{2}}$$

$$\cos\theta = \frac{1-\tan^2\frac{\theta}{2}}{1+\tan^2\frac{\theta}{2}}$$

$$\therefore \frac{\rho g}{6\gamma}R^2 = \frac{\tan^2\frac{\theta}{2}(1+\tan^2\frac{\theta}{2})}{3\tan^2\frac{\theta}{2}+1}$$

Therefore, the relationship between the radius of spherical crown and bubble contact angle

can be calculated by the equation $\boldsymbol{R^2 = \frac{6\gamma}{\rho g}\frac{\tan^2\theta/2\left(1+\tan^2\theta/2\right)}{3\tan^2\theta/2+1}}$.

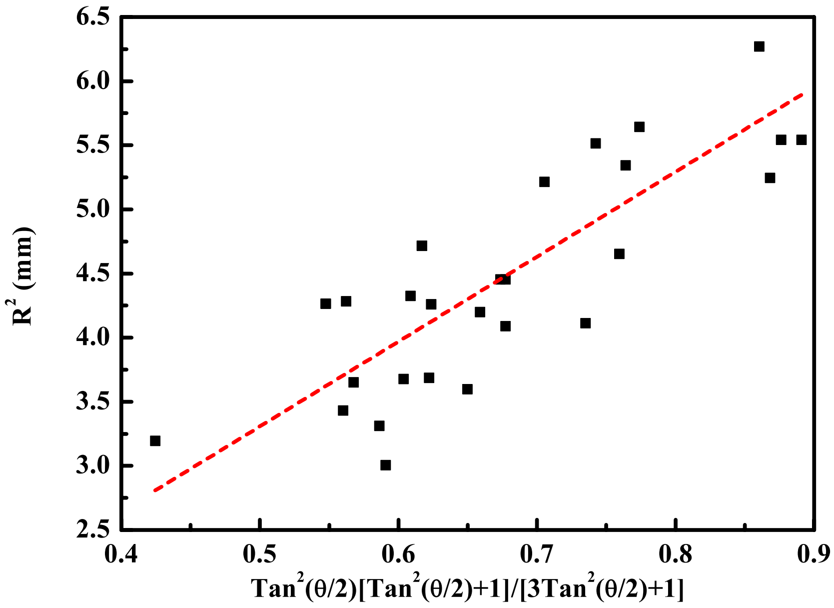

Figure S17 Variation of $\boldsymbol{R}^2$ with $\dfrac{\tan^2\theta/_2\left(1+\tan^2\theta/_2\right)}{3\tan^2\theta/_2+1}$.

According the photographs of spherical crown at equilibrium states, the variation of $\boldsymbol{R}^2$ with $\dfrac{\tan^2\theta/_2\left(1+\tan^2\theta/_2\right)}{3\tan^2\theta/_2+1}$ can be illustrated in Figure S18. It was found that the experimental data fitted well with the theoretical calculation.

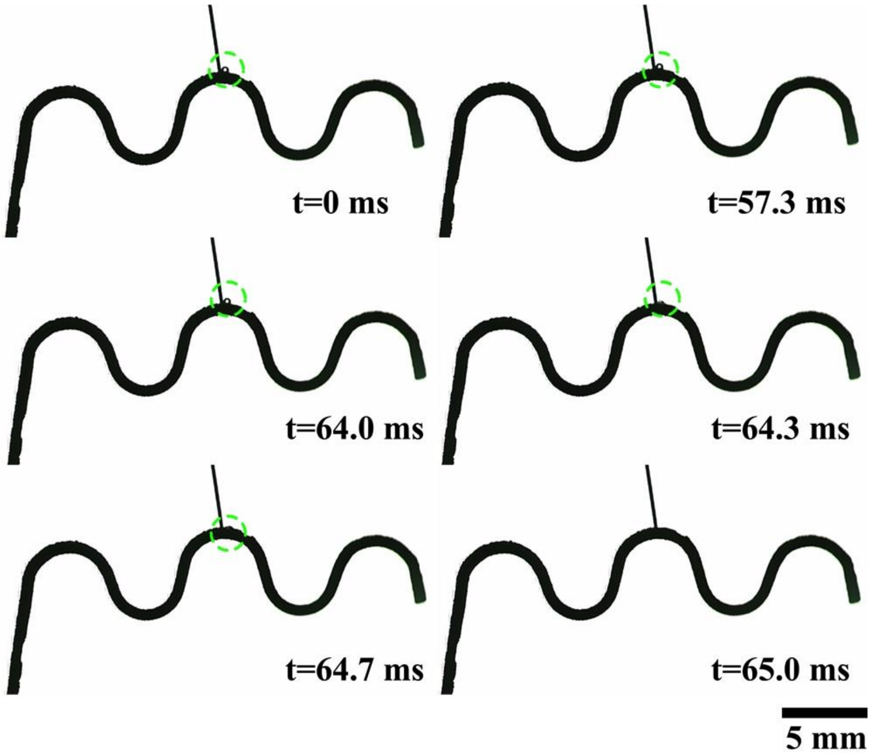

Figure S18 The absorption process of a tiny gas bubble ($\boldsymbol{R_b < 2R_w}$) when $\boldsymbol{\Delta P_b > \Delta P}$